

Received March 29, 2021, accepted April 14, 2021, date of publication April 19, 2021, date of current version April 27, 2021.

Digital Object Identifier 10.1109/ACCESS.2021.3073989

# A Minimally Configured Hardware-In-the-Loop Simulator of Electrical Power Steering System for Human Driver Interaction on Crosswind Effect

DAEYI JUNG 

School of Mechanical and Automotive Engineering, Kunsan National University, Gunsan 54150, South Korea

e-mail: dyjung@kunsan.ac.kr

This work was supported in part by the Korea Technology Evaluation and Planning (KETEP) as Human Resources Development Programs under Grant 20194010201800, and in part by the Ministry of Trade, Industry and Energy, an Industrial Technology Innovation Project, “Development for Steering Thrust 3,500kgf Class Integrated Electric Power Steering System (MDPS),” under Project P0013843.


**ABSTRACT** The advancement of electrical power steering system (EPSS) in a vehicle system has moved forward for decades. However, before the era of the complete autonomous vehicles comes, many investigations are still underway to improve EPSS characteristics and performance for the human driver interactions, while conducting both actual field tests and indoor HILS. Meanwhile, to replace the costly and time-consuming field tests, the indoor EPSS based HILS has been frequently used as an alternative to explore the characteristics of an actual EPSS and mimic the steering reaction torque created by a real car. However, the recent EPSS Hardware-In-the-Loop (HIL) simulators become computationally expensive, complicated as well as costly by integrating several software(s) with the hardware(s). This might be extravagant for those who wish to practically implement those systems within a limited budget. Therefore, we proposed a compact, cost-effective and minimum hardware-based EPSS HIL simulator interacting with a human driver. Specifically, the dynamic models of 3-D.O.F vehicle and EPSS are constructed on the virtual environment (MATLAB/ Simulink), and the dynamic behavior of EPSS, generated by those virtual models, has been mimicked via an actual motor and delivered to actual test participants operating the simulator. The effectiveness and accuracy of the proposed simulator in conjunction with a human driver have been compared with the simulation results of certified Carsim software. In addition, for our future studies, the dynamic responses of the vehicle body and EPSS under the effect of cross-wind have been explored based on the proposed simulator and, the average of human driver’s torque to compensate for the effect has been finally addressed.

**INDEX TERMS** Hardware-In-the-Loop Simulator (HIL Simulator), electrical power steering system (EPSS), crosswind effect, vehicle dynamics, motor control, steering torque, Carsim.

## I. INTRODUCTION

One of the major components of the vehicle system is EPSS, which interacts with the drivers and reduces one’s driving effort. Therefore, the advancement of EPSS in a vehicle system has moved forward for decades. The study [1] investigates the mathematical model and characteristic curves of EPSS and, explored the performance of three cases, the mechanical steering without power system, EPS system as well as EPS system with PID control, in MATLAB/Simulink environmental. In [2], a robust control design is proposed for the EPS system with a brushed motor, which consists of a

two-controllers structure. One is a robust master controller, so called “motion controller” to deal with the driver’s feeling and another is a slaver PI controller for generating sufficient assisting torque based on the command via the master motion controller. Reference [3] explored the performance of an optimal based EPS system with a brushed motor and similar control structure of [2]. Reference [4] introduced an algorithm for steering rack force estimation using a non-linear friction compensation module and a linear disturbance observer. The performance of estimation algorithm is validated with numerical EPS model, a steering test bench as well as a real prototype car. Reference [5] thoroughly reviews the overview of model-based EPSS, mainly focusing on vehicle-driver interactions and the design of a model-based EPS controller that considers

The associate editor coordinating the review of this manuscript and approving it for publication was Nasim Ullah .

the driver's characteristics. Reference [6] presents the modeling, control and analysis of an axle parallel electric power steering system used for autonomous driving through a state space approach. The control system is designed based on LQI (Linear Quadratic Integrator) with pole placement technique. Reference [7] shows that the effect of EPS (Electrical Power Steering) obviously improves steering portability and flexibility of the vehicle through the simulation results in Matlab/Simulink. Furthermore, [8] presents an adaptive global fast sliding mode control (AGFSMC) for Steer-by-Wire system vehicles with unknown steering parameters. To deal with such unknown parameters, the cooperative adaptive sliding mode observer (ASMO) and Kalman filter (KF) are designed to simultaneously estimate the vehicle states and cornering stiffness coefficients. And then, based on the best set of estimated dynamics, the proposed AGFSMC estimates the uncertain SBW system parameters and performs the robust control of system. Reference [9] constructed an accurate multi-body dynamics model of a vehicle on ADAMS/Car and explored the steering return-ability of a given model. Through the sensitivity analysis based on DOE, it is found that wheel alignment such as camber, caster and toe is one of the most important factors for the difference between left and right return forces, and rack friction has a significant influence on the remaining angle. Reference [10] proposed a nonlinear control of steering wheel angle taking advantage of the self-aligning torque for EPS in the lateral motion control of autonomous vehicles. It shows that the self-aligning torque provides the damping that can improve the tracking performance when following the same direction of the input torque on the control of steering wheel. In addition, EPS hardware-in-the-loop simulation is utilized to evaluate the performance of the proposed method. Reference [11] introduced an integrated electric power steering system (EPS) mounted on a steering column and operating with a steering gear. The outcomes of the theoretical analysis were compared with the results of tests obtained from a specially built research bench completely reflecting the work of assistance in the vehicle system. Reference [12] presents a control technique for Electric Power Steering System (EPS) using Permanent Magnet Synchronous motor (PMSM) for steering application. The mathematical model of EPS is developed in Matlab/Simulink and the performance of proposed EPS system is evaluated for different driving conditions. Reference [13] presents an overview of dynamics equation of EPS and how the EPS can be applied into large vehicle and addresses that the booster position of the motor will affect the characteristics of the overall dynamic motion of the electric power steering system. Reference [14] presents a comparative analysis of three different motor structures designed for an EPSS, the existing Interior Permanent Magnet Synchronous Motor (IPMSM), PMSM with a different rotor structure (V-shape design) as well as a synchronous reluctance machine (SynRM). Reference [15] developed a hardware-in-the-loop simulation (HILS) system and confirmed that the steering forces obtained through the simulation together with the

developed HILS system are similar to those in real vehicle tests. Reference [16] proposed a motor model-based observer to estimate the total torque on the motor shaft in the event of the torque sensor failure on EPS. And a Hardware-in-the-loop (HIL) simulation, including the EPS model, road vehicle dynamics, and the control scheme on an Opal RT real-time platform, has been conducted. Beside of the study for the performance, the design and the control of EPSS, the EPSS based lateral disturbance control has been discussed in [17] through [19]. Reference [17] addressed the control strategy using the overlay torque of assistant motor as a control input which improves the behavior of human steering under the lateral disturbance, a cross-wind effect and a road bank angle. Reference [18] deals with an estimator of lateral disturbance for an application to a EPSS-based driving assistant system. Reference [19] discussed the effectiveness of proposed lateral compensation algorithm based on a fully-equipped simulator interacting with a human driver. Based on the reviews of EPSS control system, as seen in [1]–[9], and HILS for EPSS, as shown in [10], [15], [16], [19], we recently found that the HIL simulators for EPSS becomes complicated as well as expensive by integrating several software(s) with the hardware(s). Such systems are often extravagant to explore only steering reaction torque for a human driver together with the dynamic response of the vehicle system. Therefore, we proposed a compact, cost-effective and simplified EPSS HIL simulator interacting with a human driver and, explored the characteristics of EPSS based on the proposed simulator. Specifically, the dynamic models of 3-D.O.F vehicle and steering wheel-motor-rack based EPSS are constructed virtually in Simulink, and the steering feeling (reaction torque) generated by those virtual dynamic models has been mimicked via an actual motor and delivered to actual test participants. Therefore, the extension of this simulator can be limitless due to the fact that the vehicle and EPSS dynamic models are constructed in the virtual environment and the actual motor employed here only generates the driver's reaction torque. In addition, the dynamic responses of the vehicle body and EPSS under the effect of cross-wind have been explored based on the proposed simulator for our future studies. Therefore, three major contributions of this study can be stated here. 1) we proposed a compact, cost-effective, and simplified EPSS HIL simulator interacting with a human driver where others might build at low cost along with a certain level of accuracy. 2) Based on the proposed EPSS HIL simulator, we explored the cross-wind effect on the dynamic responses of the vehicle and EPSS together with an effort of a human driver. 3) The consumed average torque of motor in EPSS has been approximately examined for the steady-state crosswind effect. The rest of paper is followed. Section.II presents the 3-D.O.F mathematical model of vehicle together with Dug-off tire model and cross-wind effect while Section.III introduces the dynamic model of EPSS. Section.IV proposed a simulator and Section.V addressed the control of actual motor and, Section.VI discussed the simulation and experimental results. Finally, the conclusions are remarked.

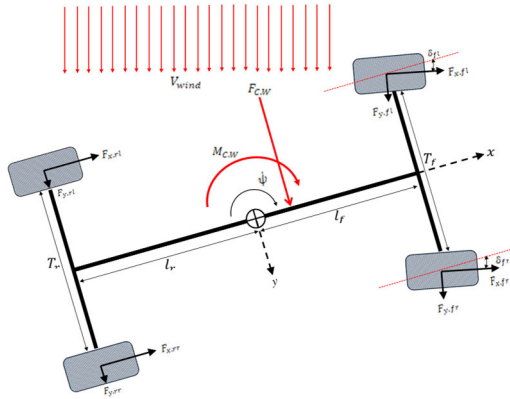


FIGURE 1. 3-D.O.F four-wheels vehicle description with a cross-wind effect.

## II. MATHEMATICAL MODELS OF VEHICLE AND TIRE WITH CROSS-WIND EFFECT

This section describes the mathematical model of the vehicle together with the cross-wind effect. The selected model is a 3-D.O.F four-wheeled vehicle, shown in Fig. 1, and implemented to dynamically interact with the dynamic model of EPSS (which will be shortly introduced in next section).

The equations of motions for the vehicle body are given by,

$$m(\dot{v}_x - \dot{\psi}v_y) = \sum F_{x,i} \quad (1)$$

$$m(\dot{v}_y + \dot{\psi}v_x) = \sum F_{y,i} + F_{C,W} \quad (2)$$

$$I_z\ddot{\psi} = \sum M_{z,i} + M_{C,W} \quad (3)$$

where,  $v_x$  and  $v_y$  are the longitudinal and lateral velocities with respect to the body-fixed frame ( $x, y$ ), respectively and,  $\dot{\psi}$  is the yaw rate of vehicle body. Also,  $m$  and  $I_z$  are vehicle mass and the moment of inertia, and  $F_{C,W}$  and  $M_{C,W}$  are the representative effective force and moment acting upon the vehicle due to the effect of cross-wind and followed as:

$$F_{C,W} = \frac{1}{2}\rho_{air}C_D A_{side}V_{C,W}^2 \quad \& \quad M_{C,W} = F_{C,W}l_{c_w} \quad (4)$$

$$V_{C,W} = V_{wind}^2 + v_x^2 - 2v_x V_{wind}\cos\left(\frac{\pi}{2} - \psi\right) \quad (5)$$

where,  $\rho_{air}$ ,  $C_D$ ,  $A_{side}$ ,  $V_{wind}$ , and  $l_{c_w}$  are respectively the air density, the drag coefficient, the effective side area for the vehicle, the speed of cross-wind as well as the relative distance to C.G where  $F_{C,W}$  is acting on.

Next,  $\sum F_{x,i}$ ,  $\sum F_{y,i}$  and  $M_{z,i}$  in (1) through (3) indicate the tire/road forces and the rotational moments, which are expressed by,

$$\sum F_{x,i} = \mathbf{u}_c \cdot \mathbf{F}_{x,f} - \mathbf{u}_s \cdot \mathbf{F}_{y,f} + \mathbf{F}_{x,r} \quad (6)$$

$$\sum F_{y,i} = \mathbf{u}_s \cdot \mathbf{F}_{x,f} + \mathbf{u}_c \cdot \mathbf{F}_{y,f} + \mathbf{F}_{y,r} \quad (7)$$

$$\begin{aligned} \sum M_{z,i} = & l_f(\mathbf{u}_s \cdot \mathbf{F}_{x,f} + \mathbf{u}_c \cdot \mathbf{F}_{y,f}) \\ & + \frac{T_f}{2}(\mathbf{u}_s^- \cdot \mathbf{F}_{y,f} + \mathbf{u}_c^- \cdot \mathbf{F}_{x,f}) - l_r \mathbf{F}_{y,r} \\ & - \frac{T_r}{2}(\mathbf{F}_{x,rr} - \mathbf{F}_{x,rl}) + [T_{S.A.T,r} + T_{S.A.T,l}] \quad (8) \end{aligned}$$

where  $\mathbf{u}_c = [\cos(\delta_{fr})\cos(\delta_{fl})] \in \mathbb{R}^{1 \times 2}$ ,  $\mathbf{u}_s = [\sin(\delta_{fr})\sin(\delta_{fl})] \in \mathbb{R}^{1 \times 2}$ ,  $\mathbf{u}_c^- = [-\cos(\delta_{fr})\cos(\delta_{fl})] \in \mathbb{R}^{1 \times 2}$  and  $\mathbf{u}_s^- = [\sin(\delta_{fr}) - \sin(\delta_{fl})] \in \mathbb{R}^{1 \times 2}$ .

Also,  $\mathbf{F}_{x,f} = [F_{x,fr} F_{x,fl}]^T \in \mathbb{R}^{2 \times 1}$ ,  $\mathbf{F}_{y,f} = [F_{y,fr} F_{y,fl}]^T \in \mathbb{R}^{2 \times 1}$ ,  $\mathbf{F}_{x,r} = [F_{x,rr} F_{x,rl}]^T \in \mathbb{R}^{2 \times 1}$  and  $\mathbf{F}_{y,r} = [F_{y,rr} F_{y,rl}]^T \in \mathbb{R}^{2 \times 1}$ . Here, the above sub-notations  $fr, fl, rr$ , and  $rl$  represent the front-right, the front-left, the rear-right and the rear-left in the four wheels of vehicle. Also,  $\delta_{fr}$  and  $\delta_{fl}$  are the front right and the left steering angles. And,  $l_f$  and  $l_r$  indicate the distance from C.G to the front axle and the one from C.G to the rear axle while  $T_f$  and  $T_r$  do the lengths of the front axle and the rear axle, as shown in Fig. 1.

In addition,  $T_{S.A.T,r}$  and  $T_{S.A.T,l}$  shown in (8) indicate the self-alignment torques (S.A.Ts) for each front tire and are followed as,

$$\begin{aligned} T_{S.A.T,r} &= \zeta C_{yy} \left( \frac{v_y}{v_x} + \frac{l_f}{v_x} \dot{\psi} - \delta_{fr} \right) \\ T_{S.A.T,l} &= \zeta C_{yy} \left( \frac{v_y}{v_x} + \frac{l_f}{v_x} \dot{\psi} - \delta_{fl} \right) \quad (9) \end{aligned}$$

where,  $\zeta$  is the trail length of front tire. Here, the S.A.Ts of rear tires are disregarded due to the effectiveness.

Furthermore, the tire model of vehicle we selected for this study is the Dug-off model due to the reasons that the formulation is close to linear and the number of parameters is relatively fewer compared to other tire models such as Pacejka tire model.

Hence, the mathematical models of each tire force are given by,

$$\begin{aligned} F_{x,i} &= C_{xx} \frac{\lambda_i}{1 - \lambda_i} k_i \quad \& \quad F_{y,i} = C_{yy} \frac{\tan \alpha_i}{1 - \lambda_i} k_i \\ \text{for } i &= fr, fl, rr, rl \quad (10) \end{aligned}$$

with,

$$k_i = \begin{cases} (2 - \sigma_i) \sigma_i & \text{if } \sigma_i < 1 \\ 1 & \text{if } \sigma_i \geq 1 \end{cases} \quad (11)$$

$$\sigma_i = \frac{(1 - \lambda_i)\mu_i F_{ni}}{2\sqrt{C_{xx}^2 \lambda_i^2 + C_{yy}^2 \tan^2 \alpha_i}} \quad (12)$$

where  $C_{xx}$  and  $C_{yy}$  are the constant longitudinal and lateral stiffness of tires and  $\mu_i$  is the friction coefficient of tire/road. Also,  $\lambda_i$  and  $\alpha_i$  indicate the longitudinal and lateral slip of each tire, computed by,

$$\lambda_i = \frac{Rw_i - v_{px,i}}{\max(Rw_i, v_{px,i})} \quad \& \quad \alpha_i = \delta_i - \tan^{-1}\left(\frac{v_{py,i}}{v_{px,i}}\right) \quad (13)$$

where  $R$  is the effective radius of tire and  $w_i$  is the angular rate of each wheel.

Also,  $v_{px,i}$  and  $v_{py,i}$  represent the linear velocities for the center of each tire and calculated by,

$$[v_{px,i} \ v_{py,i} \ 0] = [v_x \ v_y \ 0] + [0 \ 0 \ \dot{\psi}] \times [l_{x,i} \ l_{y,i} \ 0] \quad (14)$$

where  $l_{x,i}$  and  $l_{y,i}$  are the  $x$  and  $y$  positions of each tire relative to the C.G of vehicle.

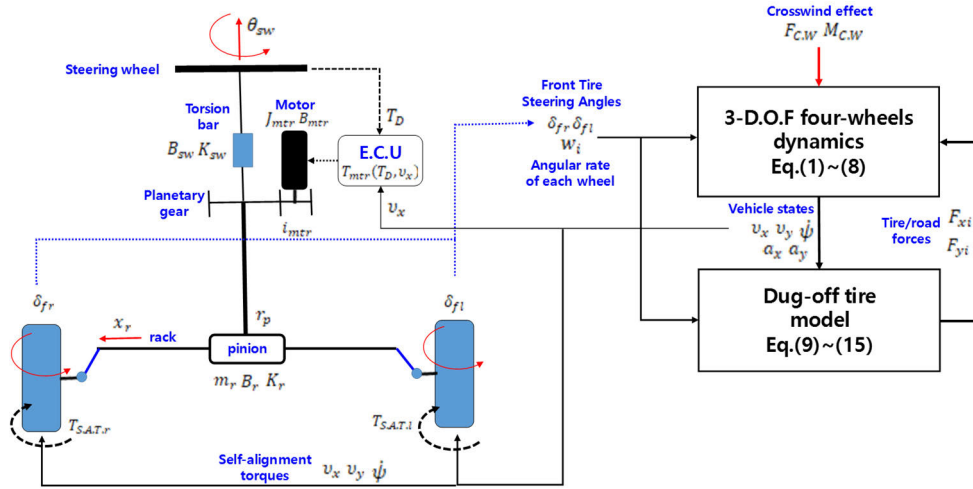


FIGURE 2. EPSS in conjunction with vehicle model.

The vertical forces ( $F_{n,i}$ ) applied to each tire can be obtained as follows,

$$\begin{aligned} F_{nfl} &= \frac{l_r mg}{2(l_f + l_r)} - \frac{hma_x}{2(l_f + l_r)} - \frac{l_r hma_y}{(l_f + l_r)} \\ F_{nfr} &= \frac{l_r mg}{2(l_f + l_r)} - \frac{hma_x}{2(l_f + l_r)} + \frac{l_r hma_y}{(l_f + l_r)} \\ F_{nrl} &= \frac{l_r mg}{2(l_f + l_r)} + \frac{hma_x}{2(l_f + l_r)} - \frac{l_r hma_y}{(l_f + l_r)} \\ F_{nrr} &= \frac{l_r mg}{2(l_f + l_r)} + \frac{hma_x}{2(l_f + l_r)} + \frac{l_r hma_y}{(l_f + l_r)} \end{aligned} \quad (15)$$

where,  $h$  is the height of C.G in the vertical direction. Both  $a_x$  and  $a_y$  in (15) are obtained via  $\dot{v}_x - \dot{\psi}v_y$  and  $\dot{v}_y + \dot{\psi}v_x$ . Also, based on the state of the vehicle in (1) through (3), the global trajectory of vehicle,  $x_G(t)$  and  $y_G(t)$ , can be computed by,

$$\begin{aligned} x_G(t) &= \int_{t_0}^t (v_x \cos(\psi) - v_y \sin(\psi)) dt \\ &\quad \& \\ y_G(t) &= \int_{t_0}^t (v_x \sin(\psi) + v_y \cos(\psi)) dt \end{aligned} \quad (16)$$

### III. DYNAMIC MODEL OF EPSS MODEL

This section deals with the dynamic model of EPSS for the proposed simulator. The simplified structure of EPSS is presented in the left of Fig. 2, and the interaction between EPSS and vehicle model is also described in Fig. 2. Specifically, the steering angles of the front tires,  $\delta_{fr}$  and  $\delta_{fl}$ , are delivered to the vehicle system from EPSS and, at same time, the states (i.e.  $v_x$ ,  $v_y$  and  $\dot{\psi}$ ) of vehicle are recursively conveyed to EPSS for determining the desired assisting torque of a motor and the S.A.Ts of tires.

Furthermore, the E.O.M of EPSS is given below. (17) represents the dynamics of steering wheel to steering column while (18) and (19) describe the part of assisting motor and the rack-pinion one. And, (20) and (21) indicate the kinematic relationship between the rack displacement and the

front-steering angles.

$$J_{sw} \ddot{\theta}_{sw} = -B_{sw} \dot{\theta}_{sw} - K_{sw} (\theta_{sw} - x_r / r_p) + T_D \quad (17)$$

$$\begin{aligned} J_{mtr} \ddot{\theta}_{mtr} &= -B_{mtr} \dot{\theta}_{mtr} + T_{mtr}(T_D, v_x) \cdots \\ &\quad - K_{mtr} (\theta_{mtr} - i_{mtr} x_r / r_p) \end{aligned} \quad (18)$$

$$\begin{aligned} m_r \ddot{x}_r &= -B_r \dot{x}_r - K_r x_r + \frac{1}{r_p} \left[ K_{mtr} \left( \frac{\theta_{mtr}}{i_{mtr}} - \frac{x_r}{r_p} \right) \right. \\ &\quad \left. + \cdots + K_{sw} \left( \theta_{sw} - \frac{x_r}{r_p} \right) \right] \\ &\quad + \frac{1}{H} [T_{S.A.T.r} + T_{S.A.T.l}] \end{aligned} \quad (19)$$

$$\delta_{fr} = \tan^{-1} \left[ \frac{(l_f + l_r) \tan(\frac{x_r}{r_p})}{(l_f + l_r) + 0.5 T_f \tan(\frac{x_r}{r_p})} \right] \quad (20)$$

$$\delta_{fl} = \tan^{-1} \left[ \frac{(l_f + l_r) \tan(\frac{x_r}{r_p})}{(l_f + l_r) - 0.5 T_f \tan(\frac{x_r}{r_p})} \right] \quad (21)$$

where,  $\theta_{sw}$  and  $\theta_{mtr}$  are respectively the rotational angles of both a steering wheel and an assisting motor. And,  $x_r$  is the transversal displacement of rack. The parameters  $B_{sw}$ ,  $B_{mtr}$ , and  $B_r$  are the viscous damping coefficients for each section. On the other hands,  $K_{sw}$ ,  $K_{mtr}$ , and  $K_r$  are the rigidity constants for each component. Also,  $i_{mtr}$  and  $r_p$  are the gear ratio of reducer and the radius of pinion-gear and,  $T_{mtr}(T_D, v_x)$  is the assistant torque provided by the motor, which is determined by the input steering torque  $T_D$  (Nm) (delivered by a driver) and the longitudinal speed of vehicle  $v_x$  (km/h).  $H$  is the equivalent length of geometric arm connected to the tie-rod/rack.

The map of target assistant torque  $T_{mtr}(T_D, v_x)$  via the motor is provided from Carsim and given in Fig. 3. Also, the simplified electrical model of motor in EPSS is described in Fig. 4 and the P.I.D controller is used to produce the target assistant torque determined by  $T_{mtr}(T_D, v_x)$ .

The parameters shown in Fig. 4 are followed.  $R_m$  ( $\Omega$ ) and  $L$  ( $\Omega s$ ) are the resistance of motor and the inductance of motor



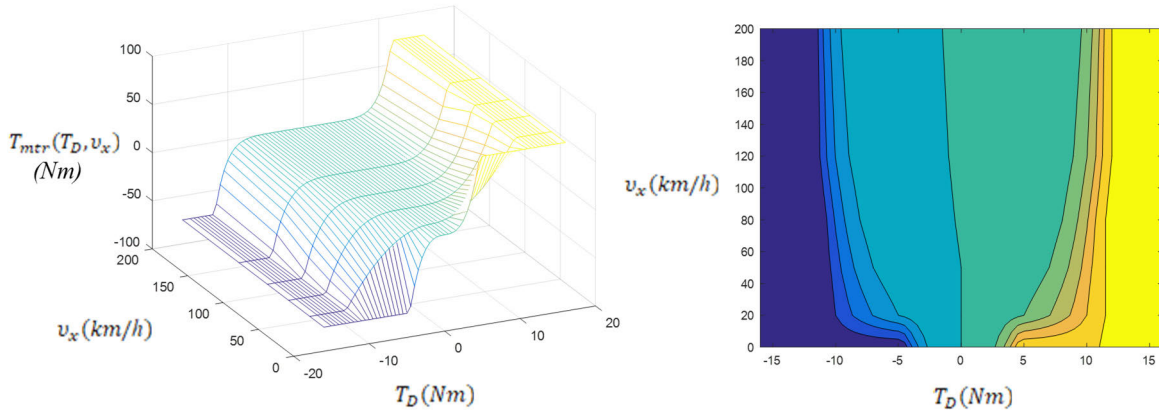


FIGURE 3. Map of target assistant torque  $T_{mtr}(T_D, v_x)$ .

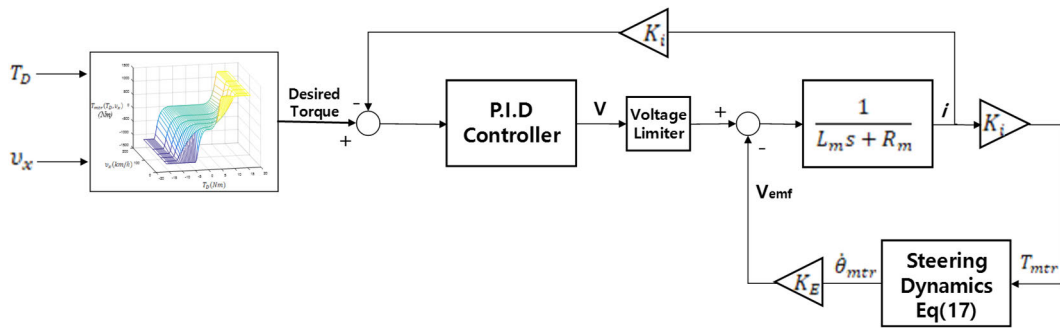


FIGURE 4. Simplified electrical model of assistant motor with P.I.D controller.

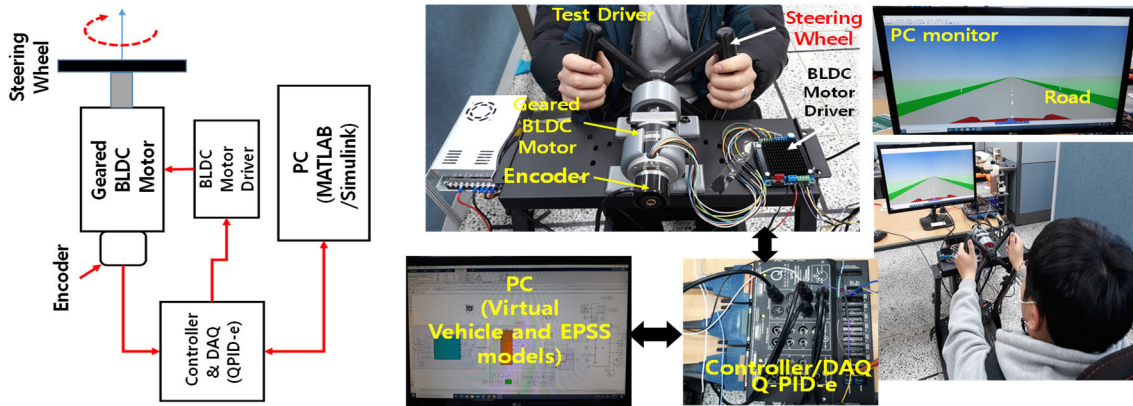


FIGURE 5. Conceptual diagram of simulator (left), an actually constructed simulator (middle), and P.C monitor for displaying the visualization of vehicle (right).

while  $K_i$  and  $K_E$  are the constant of motor ( $Nm/Amp$ ) and the constant of counter-electrical force ( $V/(rad/s)$ ), respectively.

#### IV. PROPOSED HIL SIMULATOR

The conceptual description and actual model of the proposed HIL simulator are described in Fig. 5. Compared to other simulators, this system is relatively characterized by simple and compact configuration. An inexpensive geared BLDC motor, a corresponding motor driver, a rotational

encoder sensor, a DAQ/controller(Q-PID-e), as well as a PC (MATLAB/Simulink) are major components of the simulator. The actual motor is employed to deliver the reaction torque, which is equivalent to  $T_D$  in (17), and the encoder sensor directly attached to the motor measures the rotational angle of the steering wheel, operated by a human test participant. The DAQ/controller (Q-PID-e) device controls the motor and reads the encoder simultaneously and, the vehicle and EPSS models are constructed on MATLAB /Simulink, which is

communicating with DAQ/controller(Q-PID-e). Due to the given configuration of simulator, the following sequence of the entire process can be induced. First, the BLDC motor here provides the reaction torque  $T_D$  to the driver and then the test driver delivers the steering intention (i.e, steering angle,  $\theta_{sw}$ ) against  $T_D$  created by the motor. Furthermore, the rotational steering angle  $\theta_{sw}$  created via a driver is measured by encoder sensor, which conveys to the models of vehicle and EPSS in the virtual environment through Q-PID-e device. Eventually, the vehicle and EPSS models generate the dynamic motion via the given steering input, and the motor creates another reaction torque which is newly felt by a driver. It should be mentioned that this system also visualizes the vehicle motion referenced to the view of driver via a P.C monitor. This visual effect allows the driver to steer the vehicle when asked to minimize the lateral deviation and, will be used for studying the reaction of human driver on the cross-wind effect.

## V. ACTUAL MOTOR CONTROL INTERACTING WITH HUMAN DRIVER FOR HIL SIMULATOR

The control of actual motor in the proposed HIL simulator (described in Fig. 5) has been discussed in this section. To implement the actual interaction between a human test driver and EPSS, the physical motor should mimic the actual reaction of the steering wheel.

Therefore, based on (17), the target torque of motor should be followed by,

$$T_D = J_{sw}\ddot{\theta}_{sw} + B_{sw}\dot{\theta}_{sw} + K_{sw}(\theta_{sw} - x_r/r_p) \quad (22)$$

Here,  $\theta_{sw}$  is obtained by an encoder attached to the motor (see Fig. 5), and recall that  $x_r$  in (22) is the displacement of rack in (19).

The mathematical model of actual motor, must generate the above target torque  $T_D$ , is given by,

$$J_M\ddot{\theta}_M + B_M\dot{\theta}_M = \tau_M(t) + T_{driver} \quad (23)$$

where,  $J_M$  and  $B_M$  are the mass inertia of actual motor and the viscous damping of motor respectively. Also,  $T_{driver}$  and  $\theta_M$  are respectively the human reaction torque, which should meet  $T_D$ , and the actual rotational angle of motor. And, due to the given configuration of HIL simulator in Fig. 5, it is clear that  $\theta_M = \theta_{sw}$ .

The feedback control law for the target torque  $T_D$  of the motor is proposed by,

$$\tau_M(t) = \Delta J\ddot{\theta}_{sw} + \Delta B\dot{\theta}_{sw} - K_{sw}(\theta_{sw} - x_r/r_p) \quad (24)$$

where,  $\Delta J = (J_M - J_{sw})$  and  $\Delta B = (B_M - B_{sw})$ .

And then, applying (24) into (23) yields,

$$J_{sw}\ddot{\theta}_{sw} + B_{sw}\dot{\theta}_{sw} + K_{sw}(\theta_{sw} - x_r/r_p) = T_{driver} \quad (25)$$

Therefore, according to (25), the human test driver exactly experiences the desired/target reaction torque  $T_D$  (see (22)).

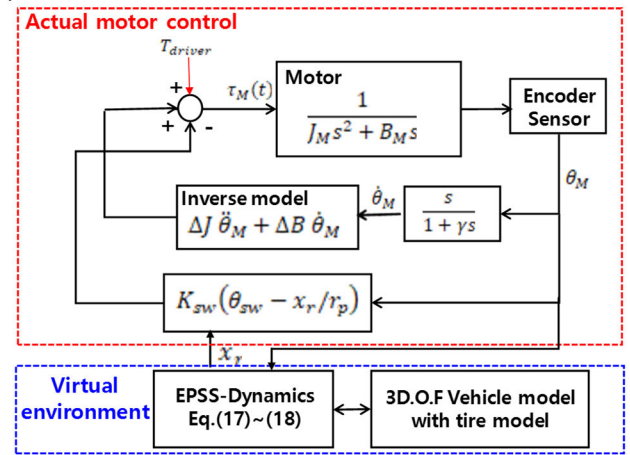


FIGURE 6. Entire control strategy of motor and interaction between the virtual dynamics and the human driver.

Assuming  $\ddot{x}_r$  and  $\dot{x}_r$  are sufficiently small, we have the following differential equation and transfer function, based on (25),

$$J_{sw}(\ddot{\theta}_{sw} - \frac{\ddot{x}_r}{r_p}) + B_{sw}(\dot{\theta}_{sw} - \frac{\dot{x}_r}{r_p}) + K_{sw}(\theta_{sw} - x_r/r_p) = T_{driver} \quad (26)$$

$$e(s)/T_{driver}(s) = 1/(J_{sw}s^2 + B_{sw}s + K_{sw}) \quad (27)$$

where,  $e(s) = (\theta_{sw}(s) - x_r(s)/r_p)$ . Hence, it can be seen that the closed-loop system (27) is stable as long as the coefficient of characteristic equation are all positive (i.e,  $\max \text{Re}(s_i) < 0$  for  $i = 1, 2$ ) and  $T_{driver}$  is bounded.

The entire control strategy of motor and interaction between the virtual dynamics and the physical environment (together with the human driver) are presented in Fig. 6 for a clear understanding of the motor control in the proposed system.

## VI. SIMULATION AND EXPERIMENTAL RESULTS

This section presents the experimental results to explore the effectiveness of proposed system and the system parameters used for the study are listed in Table. 1.

In Fig. 7, the performance of the proposed system has been verified by comparing the results with the one obtained by Carsim, based on the steering wheel angle  $\theta_{sw}$  (i.e, the resultant created by human test driver who experiences the reaction torque  $T_D$ ), measured by the encoder attached to the motor in the simulator (shown in Fig. 5). Fig. 7 (b) and (c) indicate the lateral acceleration ( $a_y$ ) and the yaw rate ( $\dot{\psi}$ ) of vehicle body at the given speed  $v_x = 30\text{km/h}$  while (d) and (e) do the steering angle of front-right wheel and the steering wheel torque  $T_D$ . And, (f) represents the characteristic of motor torque for a given  $T_D$ . It can be seen that the mutual agreement between the results via simulator and the Casim's is successfully made, although a slight deviation between those two for  $T_D$  is observed. Fig. 8 and Fig. 9 also present the comparisons between the simulator's and the Carsim's for two different vehicle speeds,  $v_x = 50 \text{ km/h}$

TABLE 1. Numerical values of system parameters.

Parameters	Symbols	Values
Vehicle mass	$m$	2400kg
Moment of inertia	$I_z$	4116 kgm <sup>2</sup>
Distances between C.G and the front axle and the rear axle	$l_f$ and $l_r$	1.35 m and 1.75m
Lengths of front and rear axles.	$T_f$ and $T_r$	1.560 m and 1.560 m
Tire stiffness in longitudinal and lateral directions	$C_{xx}$ and $C_{yy}$	30000 and 60000 N/rad
Effective radius of tire	$R$	0.393 m
Damping coefficients for assisting motor and rack sections	$B_{mtr}$ , and $B_r$	0.2 and 653 Nm rad/s
Rigidity coefficients for steering wheel, assisting motor, and rack sections	$K_{sw}$ , $K_{mtr}$ , and $K_r$	115, 125, and 30000 Nm/rad
Gear ratio of reducer	$i_{mtr}$	7.25
Trail length of front tire	$\zeta$	0.025m

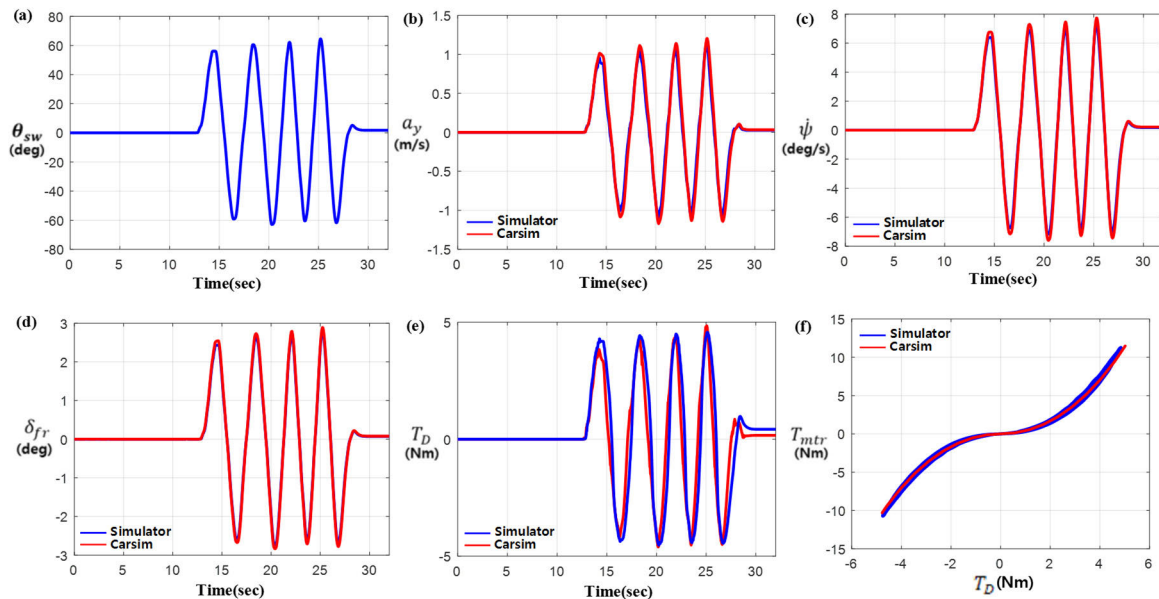
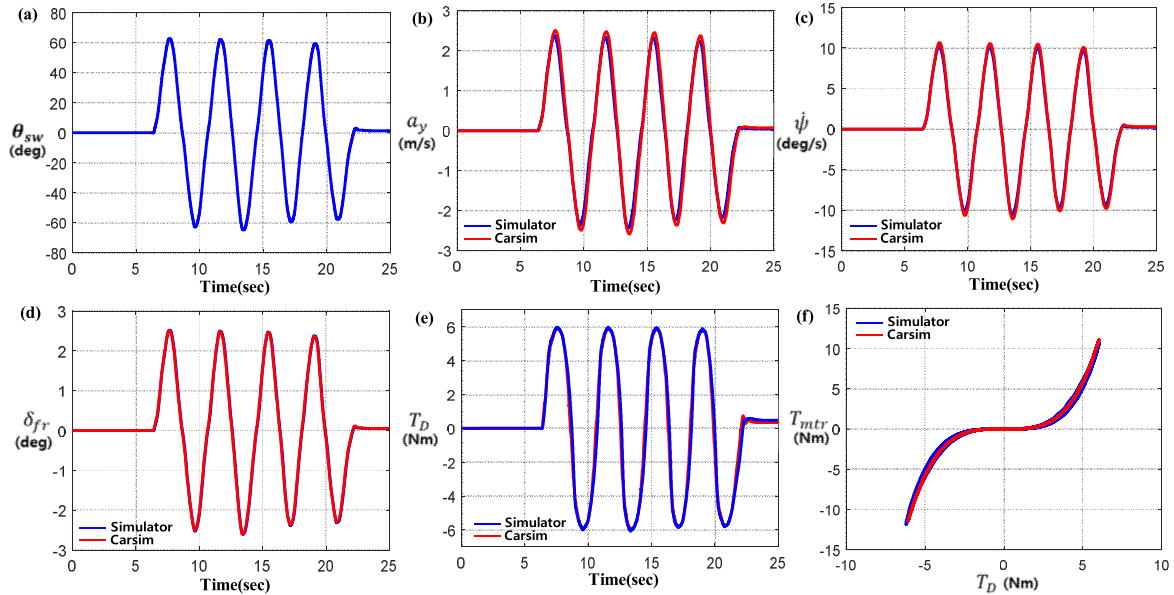


FIGURE 7. Comparison between the Carsim and the proposed simulator at  $v_x = 30\text{km/h}$  (a) Steering wheel angle (b) lateral acceleration of vehicle (c) yaw rate of vehicle (d) front steering angle on the right side (e) Torque delivered by driver (f) Torque delivered by driver vs. Assistant torque by motor in EPSS.

and  $v_x = 70 \text{ km/h}$ . It is found that those results in both Fig. 8 and Fig. 9 also exhibit acceptable mutual synchronizations between those two (simulator vs. Carsim). Nevertheless, the  $T_D$  of Carsim shows unexpected behavior that cannot be imitated by the proposed system near the inflection regions at the given  $v_x = 70\text{km/h}$  (as shown in Fig. 9(e)). Furthermore, the accuracy of S.A.T in (15) has been investigated from both Fig. 10 and Fig. 11. It is seen that the S.A.T of Carsim is well matched with the proposed one and, the S.A.T increases as the  $v_x$  does. Fig. 12(a) collected the characteristics curves of EPSS,  $T_D$  vs.  $T_{mtr}(T_D, v_x)$ , shown in Fig. 7(f), Fig. 8(f) and Fig. 9(f) and compared one with another. The human effort  $T_D$  should be increased as  $v_x$  is augmented, if an identical assistant torque is provided to each case, due to the fact that the S.A.T is augmented for larger  $v_x$ . This point of view can be seen from the results  $\theta_{sw}$  vs.  $T_D$  in Fig. 12(b). It is clear that the human test driver generates an almost identical range of

steering angle (approximately from  $-62 \text{ deg.}$  to  $62 \text{ deg.}$ ) for the three different vehicle speeds but consumes higher  $T_D$ s for higher speeds (i.e., max  $T_D = 4.8 \text{ Nm}$  at  $v_x = 30\text{km/h}$ , max  $T_D = 6.1 \text{ Nm}$  at  $v_x = 50\text{km/h}$ , and max  $T_D = 7.1 \text{ Nm}$  at  $v_x = 70\text{km/h}$ ). Also, it should be noted that the assistant torque  $T_{mtr}(T_D, v_x)$  consumed for three different speeds  $v_x = 30, 50,$  and  $70 \text{ km/h}$ , are almost identical for one to another, which can be seen from Fig. 12(c) (i.e., the levels of target torque on the map are same at given range of human input torque  $T_D$ , regardless of speeds). We can see from Fig. 9 through Fig. 12 that the proposed system in this study well mimics the dynamic response of a certified Carsim.

Fig. 13 presents the global trajectories of vehicle  $(x, y)$  for two different cross-wind effects  $V_{wind} = 20\text{m/s}$  and  $V_{wind} = 30\text{m/s}$  without the human driver intervention (i.e.,  $T_d = 0$ ) at the speeds  $v_x = 50 \text{ km/h}$  and  $v_x = 70 \text{ km/h}$ . It is



**FIGURE 8.** Comparison between the Carsim and the proposed simulator at  $v_x = 50 \text{ km/h}$  (a) Steering wheel angle (b) lateral acceleration of vehicle (c) yaw rate of vehicle (d) front steering angle on the right side (e) Torque delivered by driver (f) Torque delivered by driver vs. Assistant torque by motor in EPSS.

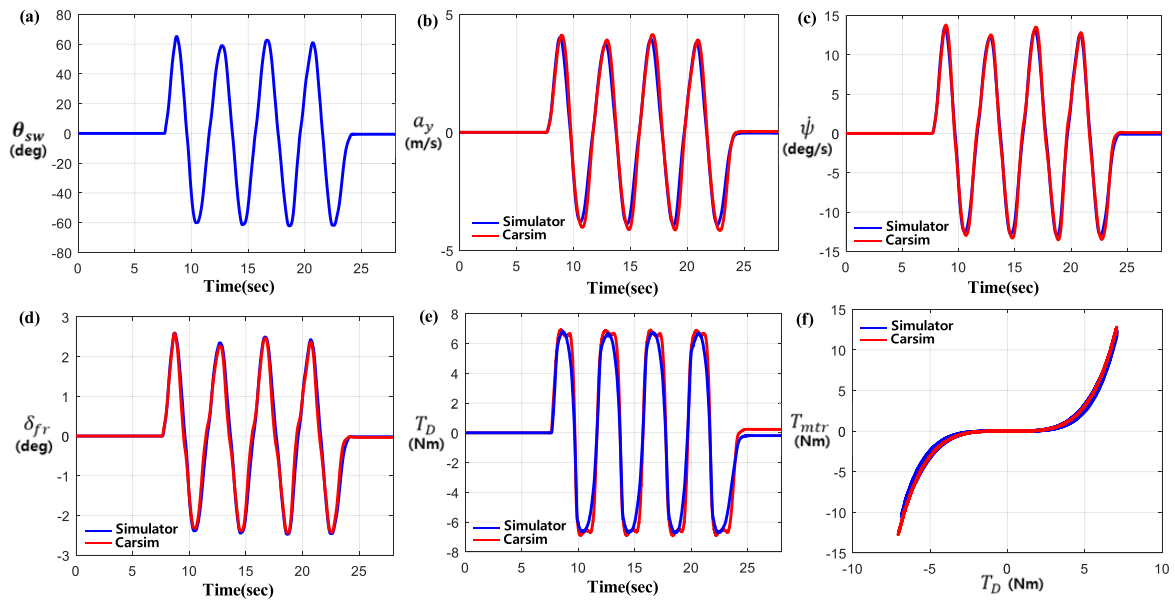


**FIGURE 9.** Comparison between the Carsim and the proposed simulator at  $v_x = 70 \text{ km/h}$  (a) Steering wheel angle (b) lateral acceleration of vehicle (c) yaw rate of vehicle (d) front steering angle on the right side (e) Torque delivered by driver (f) Torque delivered by driver vs. Assistant torque by motor in EPSS.

assumed here that there exist no other road disturbances. Therefore, from the results of Fig. 13, we can explore the pure effect of cross-wind on the vehicle system. Specifically, the constant cross-wind has been blown to the side of vehicle since 10 secs, as shown in Fig. 13(a). Hence, we can see that the vehicle has moved straightly before 10 secs (no cross-wind effect) and then deviated from the originally intended path line after 10 secs. It can also be seen that, as generally predicted, the effect of strong winds produces

larger lateral deviations. The percentages of final lateral deviation, defined as the ratio between the longitudinal distance and the lateral distance, are approximately 4 ~ 5% for  $V_{wind} = 20 \text{ m/s}$  and 11 ~ 15% for  $V_{wind} = 30 \text{ m/s}$ , which can be characterized by a huge lateral disturbance. Fig. 13 also includes the performance comparison between the simulator and Carsim and, it is clear that the trajectory of vehicle created by the proposed simulator is well synchronized with Carsim's.



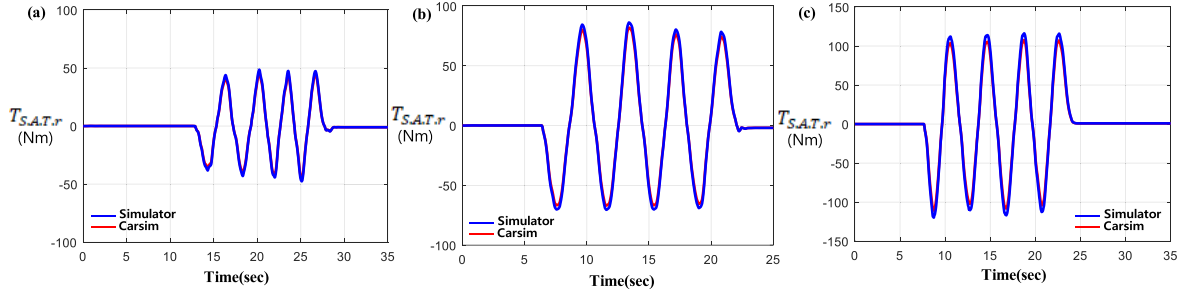


FIGURE 10. Self-aligned torque in the left wheel for three different velocities  $v_x = 30, 50, 70$ km/h (a) S.A.T at 30km/h, (b) S.A.T at 50km/h, (c) S.A.T at 70km/h.

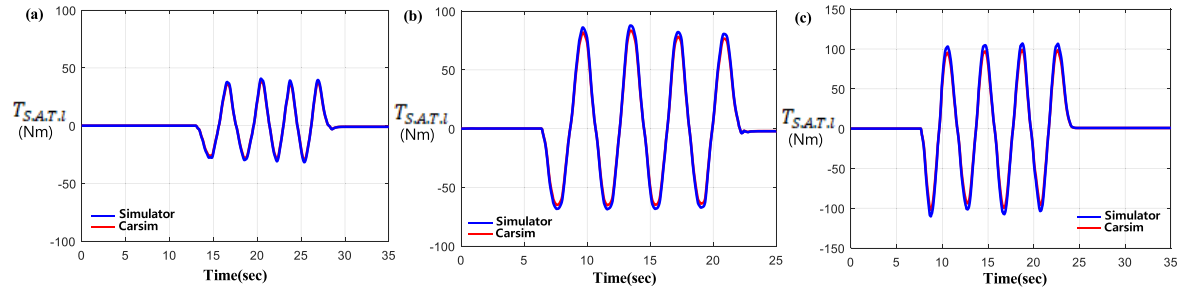


FIGURE 11. Self-aligned torque in the right wheel for three different velocities  $v_x = 30, 50, 70$ km/h (a) S.A.T at 30km/h, (b) S.A.T at 50km/h, (c) S.A.T at 70km/h.

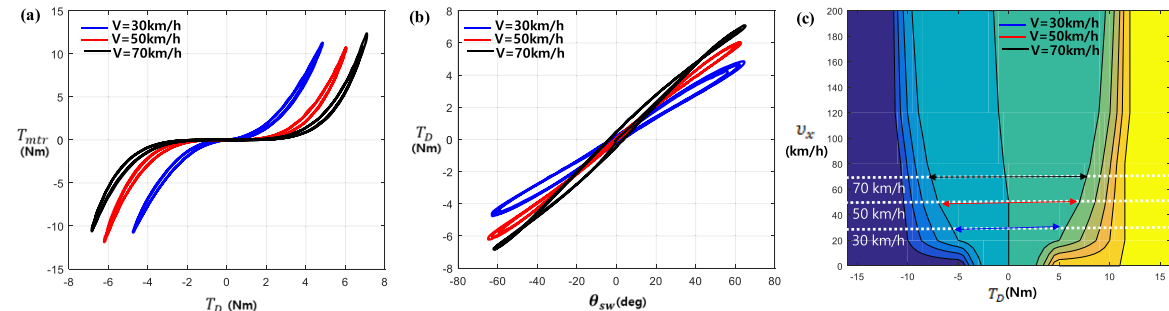
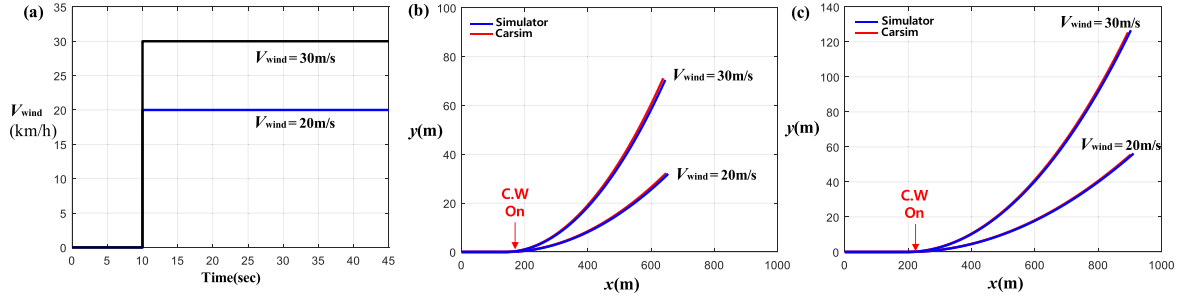


FIGURE 12. Characteristics of EPSS for three different velocities  $v_x = 30, 50, 70$ km/h (a) Torque delivered by driver vs. Assistant torque by motor in EPSS (b) Torque delivered by driver vs. Steering wheel angle (c) Torque used according to the target torque map for the different speeds.

Fig. 14 shows the responses of proposed system under a human driver intervention for the cross-wind effect  $V_{wind} = 30$ m/s at a given vehicle speed  $v_x = 50$ km/h. Fig. 14(a) through (d) represent the yaw rate of vehicle body, the global y-trajectory of vehicle, the torque delivered by a driver and the steering wheel angle on the time domain. Here, the cross-wind is imposed on vehicle model at 3 secs and a human test driver is requested to steer the vehicle against the cross-wind effect at 23 secs, where the vehicle is significantly deviated from the originally intended straight path line.

Therefore, as shown in Fig. 14(a) and (b), the yaw rate and y-trajectory of vehicle body are induced from 3 secs to

23 secs due to the cross-wind effect. Next, when the driver is requested to maneuver the vehicle on a zero deviation of the lateral trajectory at 23 secs, the counter motion of the vehicle for the cross-wind effect occurs via the action of the driver. The corresponding steering wheel torque and angle are exhibited after 23 secs as shown in Fig. 14(c) and (d). This implies that the persistent steering is required to correct the heading angle of vehicle. The torque transmitted by the driver is about 4.3 Nm on average even under the assistance of a motor in EPSS, which is not negligible in terms of the driver’s effort. Fig. 15 discussed the intervention of three human test drivers for the cross-wind effect  $V_{wind} = 15$  m/s at  $v_x = 80$ km/h. Here, we categorized three drivers



**FIGURE 13.** Vehicle trajectories for two different cross wind effects  $V_{wind} = 20\text{m/s}$  and  $V_{wind} = 30\text{m/s}$  w/o the human driver's intervention (i.e.  $T_d = 0$ ) (a) Two cross-wind scenarios, (b) Vehicle trajectories at constant  $v_x = 50\text{km/h}$ , (c) Vehicle trajectories at constant  $v_x = 70\text{km/h}$ .

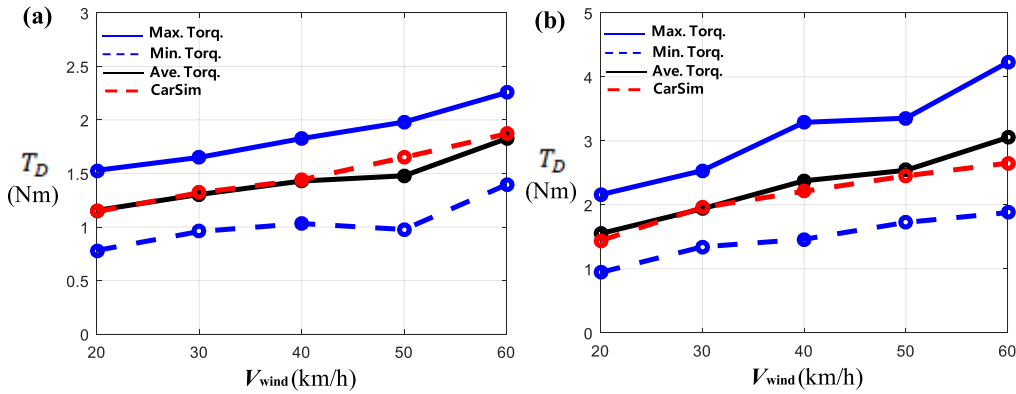


**FIGURE 16.** Average, minimum and maximum values of steady-state steering wheel torque for five different crosswind effects (three tests have been conducted for each  $V_{wind}$ ) (a) steering wheel torques @  $v_x = 60\text{km/h}$ , (b) steering wheel torques @  $v_x = 80\text{km/h}$ .

as a beginner, an intermediate and an expert based on their driving experience. It is imposed that the constant cross-wind is impacted on vehicle model at 3 secs and a human driver is requested to firmly hold the steering wheel from the beginning. As shown in Fig. 16, the responses of intermediate and expert are relatively steady and calmly for sudden wind effect while the novice exhibits a rapid steering operation resulting in a distinguishable lateral deviation. Specifically, it can be seen that the maximum steering torque and angles of novice are approximately 1.25 Nm and 3.7 degs. On the other hands, the maximum values of other drivers are less than 1 Nm and 2.3 degs. Those results imply that the effect of cross-wind might result in the dangerous situation for less experienced driver. In addition, three responses of drivers are compared with the results obtained via Carsim simulation including its own driver model (driver preview time 0.15 sec), and we can see that the steady-state of steering wheel angle and torque are quite similar to the Carsim's (even if the transient parts do not coincide with each other).

Furthermore, from Fig. 17, we can see the average, minimum, and maximum values of steady-state steering wheel torque for five different crosswind effects, 20 km/h, 30 km/h, 40 km/h, 50 km/h and 60 km/h, suddenly blown to the side of vehicle. While Fig. 16(a) indicates the results of

$v_x = 60\text{km/h}$ , Fig. 16(b) represents the outcomes for  $v_x = 80\text{km/h}$ . Here, three tests have been conducted for each  $V_{wind}$  scenario and, the corresponding average, minimum, and maximum values of  $T_D$  have been expressed in Fig. 16. Especially, it can be seen that the average values are well synchronized with the Carsim's. According to Fig. 16, the constant human effort for the crosswind effect requires at least 1 ~ 4 Nm. This will be important data for determining the assistant torque of motor in the lateral disturbance compensation system which is our next study. Based on the results in Fig. 15 and Fig. 16, it can be said that the performance of proposed simulator acceptably captures the essence of human effort for the steady-state crosswind effect.

Also, based on the results in Fig. 15 and Fig. 16, the overlay assistant torque of motor can be determined to minimize human effort for the crosswind effect. The steady-state conditions of (17) and (18) are given by,

$$\frac{x_r}{r_p} = \theta_{sw} - T_D/K_{sw} \tag{28}$$

$$T_{mtr} = K_{mtr} (\theta_{mtr} - i_{mtr}x_r/r_p) \tag{29}$$

Substituting (28) into (29) yields,

$$T_{mtr} = K_{mtr} (\theta_{mtr} - i_{mtr}\theta_{sw}) + i_{mtr} \frac{K_{mtr}}{K_{sw}} T_D \tag{30}$$

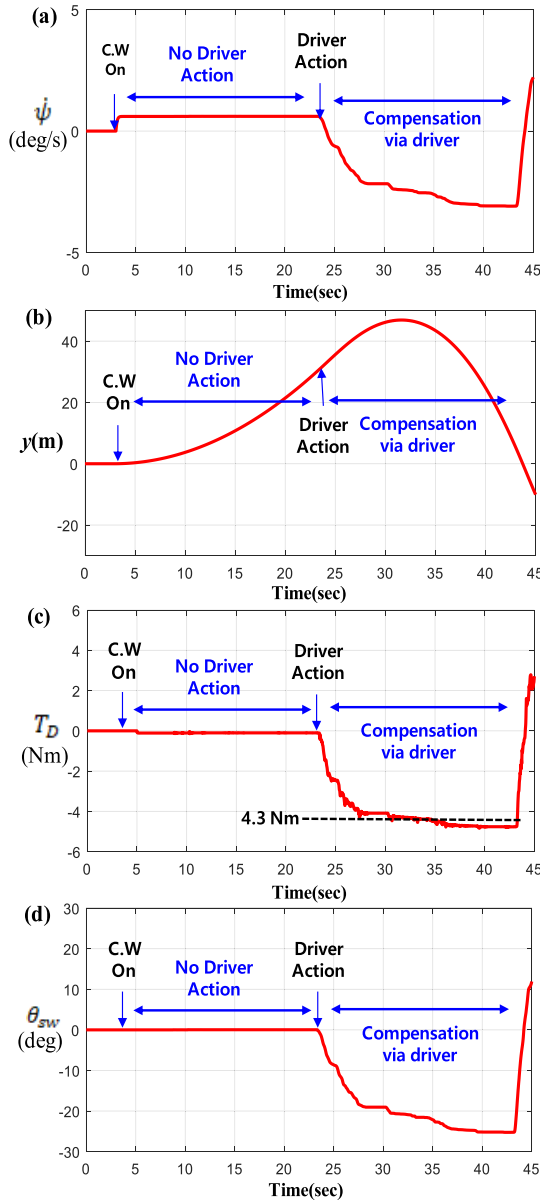


**FIGURE 14.** System responses under human driver intervention for cross wind effects  $V_{wind} = 30\text{m/s}$  at  $v_x = 50\text{km/h}$  (The cross-wind is imposed on vehicle model at 3 secs and a human driver is requested to steer the vehicle at 23 secs) (a) yaw rate of vehicle body, (b) y-trajectory of vehicle, (c) Torque delivered by driver, (d) Steering wheel angle.

It is possible to assume that  $\theta_{mtr} \approx i_{mtr}\theta_{sw}$  and the 1<sup>st</sup> term is less dominant to the 2<sup>nd</sup> term in (30).

Hence, (30) becomes,

$$T_{mtr} \approx \alpha_s T_D \quad (31)$$

where  $\alpha_s = i_{mtr} \frac{K_{mtr}}{K_{sw}}$ . (31) determines the approximate steady-state torque of motor for given the human steering wheel torque. Therefore, to minimize the human effort for the crosswind effect, the consumed torque of motor can be approximately computed by (31). This result also leads to a guideline for the lateral compensation control system. Usually,  $\alpha_s$  is 4 ~ 5. This implies that the overlay torque of motor is approximately 4 ~ 20 Nm.

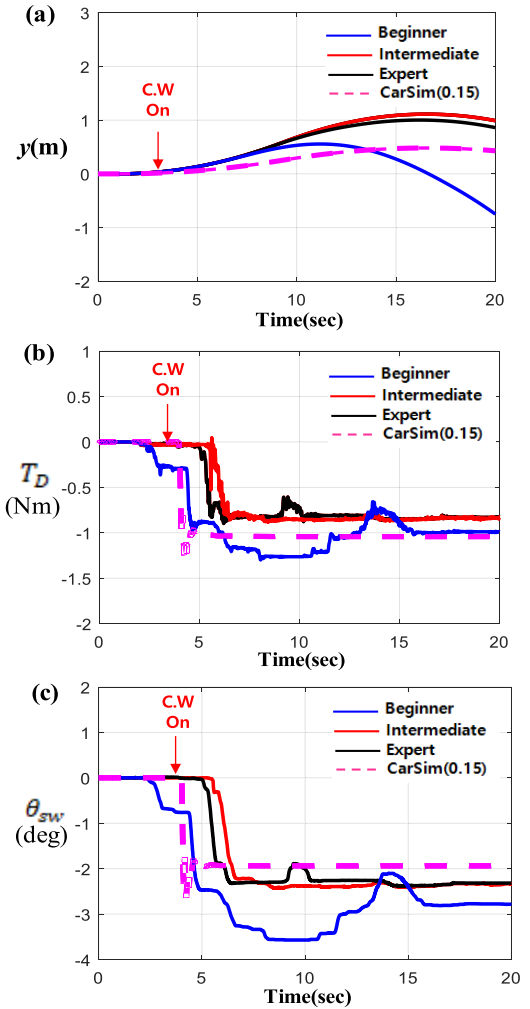


**FIGURE 15.** System responses under human driver intervention for cross wind effects  $V_{wind} = 15\text{m/s}$  at  $v_x = 80\text{km/h}$  (The cross-wind is imposed on vehicle model at 3 secs and a human driver is requested to hold the steering wheel from the beginning) (a) Lateral trajectory of vehicle, (b) Torque delivered by driver, (c) Steering wheel angle.

## VII. CONCLUSION

Here, we proposed a compact, cost-effective and simplified EPSS HIL simulator interacting with a human driver and, explored the characteristics of EPSS and the effort of human driver under the effect of cross-wind based on the proposed simulator. Specifically, the dynamic models of 3-D.O.F vehicle and the EPSS consisting of steering wheel-motor-rack is virtually constructed in MATLAB/Simulink, and the steering feeling (reaction torque) generated by those virtual dynamic models has been mimicked via an actual motor, which is delivered to actual test participants. In addition, the cross-wind effect has been modeled and is interacted with the vehicle. It is found that the effectiveness of proposed simulator is well matched with Carsim's and an acceptable tool to investigate the effort of human driver for the cross-wind effect. Based on this system, our future study will conduct the design of compensation control system for the lateral disturbances including the cross-wind effect. This work will be a valuable asset for those who wish to construct cost-effective HIL

simulator and explore the characteristics of EPSS and human driver's intervention under one of major lateral disturbances, a cross-wind effect.

## REFERENCES

- [1] H. Zhang, Y. Zhang, J. Liu, J. Ren, and Y. Gao, "Modeling and characteristic curves of electric power steering system," in *Proc. Int. Conf. Power Electron. Drive Syst. (PEDS)*, Taipei, Taiwan, Nov. 2009, pp. 1390–1393, doi: [10.1109/PEDS.2009.5385774](https://doi.org/10.1109/PEDS.2009.5385774).
- [2] X. Chen, X. Chen, and K. Li, "Robust control of electric power-assisted steering system," in *Proc. IEEE Vehicle Power Propuls. Conf.*, Chicago, IL, USA, Sep. 2005, pp. 473–478, doi: [10.1109/VPPC.2005.1554539](https://doi.org/10.1109/VPPC.2005.1554539).
- [3] X. Chen, X. Chen, and K. Zhou, "Optimal control of electric power-assisted steering system," in *Proc. IEEE Conf. Control Appl. (CCA)*, Toronto, ON, Canada, Aug. 2005, pp. 1403–1408, doi: [10.1109/CCA.2005.1507328](https://doi.org/10.1109/CCA.2005.1507328).
- [4] S. Fankem, T. Weiskircher, and S. Müller, "Model-based rack force estimation for electric power steering," *IFAC Proc. Volumes*, vol. 47, no. 3, pp. 8469–8474, 2014.
- [5] N. Mehrabi, "Dynamics and model-based control of electric power steering systems," 2014.
- [6] V. Govender and S. Müller, "Modelling and position control of an electric power steering system," *IFAC-PapersOnLine*, vol. 49, no. 11, pp. 312–318, 2016.
- [7] Z. Ma and C. Zhan, "System stability and control strategy of electric power steering," 2015.
- [8] J. Iqbal, K. Zuhaib, C. Han, A. Khan, and M. Ali, "Adaptive global fast sliding mode control for Steer-by-Wire system road vehicles," *Appl. Sci.*, vol. 7, no. 7, p. 738, Jul. 2017.
- [9] H. Cho, B. Lee, S. Chang, Y. Park, M. Kim, and S. Hwang, "Sensitivity analysis of steering wheel return-ability at low speed," 2017.
- [10] W. Kim, C. M. Kang, Y.-S. Son, and C. C. Chung, "Nonlinear steering wheel angle control using self-aligning torque with torque and angle sensors for electrical power steering of lateral control system in autonomous vehicles," *Sensors*, vol. 18, no. 12, p. 4384, 2018, doi: [10.3390/s18124384](https://doi.org/10.3390/s18124384).
- [11] A. Kuranowski, "Electrical power steering—Modelling and bench testing," *Tech. Trans.*, vol. 8, pp. 143–158, 2019.
- [12] R. R. Hiremath and T. B. Isha, "Modelling and simulation of electric power steering system using permanent magnet synchronous motor," 2019.
- [13] N. Nazaruddin, F. Zainuri, R. Siregar, G. Heryana, M. Adhitya, and D. Sumarsono, "Electric power steering: An overview of dynamics equation and how it's developed for large vehicle," 2019.
- [14] P. P. Florin, R. Mircea, P. Adrian-Cornel, R. Martis, and C. Martis, "Comparative analysis for an electric power steering system," in *Proc. 13th Int. Conf. Electr. Mach. (ICEM)*, Alexandroupoli, Greece, Sep. 2018, pp. 590–596, doi: [10.1109/ICELMACH.2018.8507038](https://doi.org/10.1109/ICELMACH.2018.8507038).
- [15] M. H. Lee, H. M. Lee, K. S. Lee, S. K. Ha, J. I. Bae, J. H. Park, H. G. Park, H. J. Choi, and H. H. Chun, "Development of a hardware in the loop simulation system for electric power steering in vehicles," *Int. J. Automot. Technol.*, vol. 12, no. 5, pp. 733–744, Oct. 2011.
- [16] M. Lawson and X. Chen, "Hardware-in-the-loop simulation of fault tolerant control for an electric power steering system," in *Proc. IEEE Vehicle Power Propuls. Conf.*, Harbin, China, Sep. 2008, pp. 1–6, doi: [10.1109/VPPC.2008.4677453](https://doi.org/10.1109/VPPC.2008.4677453).
- [17] K. Kim, J. Choi, and K. Yi, "Lateral disturbance compensation using motor driven power steering," in *Proc. IEEE 75th Veh. Technol. Conf. (VTC Spring)*, Yokohama, Japan, May 2012, pp. 1–5, doi: [10.1109/VETECS.2012.6240282](https://doi.org/10.1109/VETECS.2012.6240282).
- [18] K. Kim, S. Lee, and C. Park, "Estimation of lateral force due to lateral disturbance for application to an MDPS-based driving assistant system," *SAE Int. J. Mater. Manuf.*, vol. 4, no. 1, pp. 1014–1024, Apr. 2011, doi: [10.4271/2011-01-0977](https://doi.org/10.4271/2011-01-0977).
- [19] K. Kim, B. Kim, Y. Go, J. Park, J. Park, I. Suh, and K. Yi, "An investigation on motor-driven power steering-based crosswind disturbance compensation for the reduction of driver steering effort," *Vehicle Syst. Dyn.*, vol. 52, no. 7, pp. 922–947, 2014, doi: [10.1080/00423114.2014.909941](https://doi.org/10.1080/00423114.2014.909941).



**DAEYI JUNG** received the Ph.D. degree from the Department of Mechanical Engineering from The University of Tennessee, Knoxville, USA, in 2012. He is currently an Associate Professor with the Department of Mechanical Engineering, Kunsan National University (KSNU), South Korea. He worked as Senior Researcher with Samsung Electronics and Hyundai-Motors for several years. Since 2017, he has been with Kunsan National University. His research interest includes control and analysis of nonlinear systems.

...